The crystallography of $M_{23}C_6$ carbides in a martensitic 9% Cr steel after tempering, aging and creep

A. Kipelova*, A. Belyakov and R. Kaibyshev

Laboratory of Mechanical Properties of Nanostructured Materials and Superalloys, Belgorod State University, Pobeda 85, Belgorod 308015, Russia

The orientation relationships of $M_{23}C_6$ carbides in a martensitic creep resistant steel were studied. Almost all $M_{23}C_6$ carbides were located at (sub)grain boundaries after tempering and aging. The carbides were slightly elongated along the boundary planes and obeyed the Kurdjumov-Sachs, Nishiyama-Wassermann, and Pitsch orientation relationships as well as two new orientation relationships, that is $(1\,1\,0)_\alpha||(1\,1\,1)_{M_{23}C_6}[0\,0\,1]_\alpha|||[4\,\bar{3}\,\bar{1}]_{M_{23}C_6}$ and $(1\,1\,0)_\alpha||(1\,1\,1)_{M_{23}C_6}[1\,\bar{1}\,\bar{1}]_\alpha|||[4\,\bar{3}\,\bar{1}]_{M_{23}C_6}$, with α-Fe matrix. On the other hand, the $M_{23}C_6$ particles in the neck portion of crept specimen lost their orientation relationships with α-Fe.

Keywords: tempering; transmission electron microscopy; martensitic steel; creep; $M_{23}C_6$ orientation relationship

1. Introduction

The 9–12% chromium creep resistant steels are used for high-temperature components in fossil power plants [1–4]. The service properties of these steels are obtained by a complex alloying that provides dispersion and solution strengthening. After tempering, the microstructure of 9–12%Cr steels consists of a tempered martensite lath structure with a fine dispersion of $M_{23}C_6$ carbides and MX carbonitrides that provides high creep strength [5,6]. The $M_{23}C_6$ carbides mainly are formed on grain and subgrain boundaries and they act as obstacles for migrating boundaries. Recently, Armaki et al. suggested that the stability of tempered martensite lath structure during creep at elevated temperatures is mainly affected by $M_{23}C_6$-type particles situated at (sub)grain boundaries [7]. The interfacial energy for $M_{23}C_6$ as calculated by DICTRA software is 0.1–0.3 J/m^2 at 650 °C [3,8]. Such small values of the interfacial energy indicate that the interfaces between $M_{23}C_6$ carbides and α-Fe should be coherent. Several works were devoted to the study of the orientation relationships in the tempered steels [9,10]. Kurdjumov-Sachs ($(0\,1\,1)_\alpha||(1\,1\,1)_{M_{23}C_6}[\bar{1}\,1\,\bar{1}]_\alpha|||[0\,1\,\bar{1}]_{M_{23}C_6}$) and Nishiyama–Wassermann ($(0\,1\,1)_\alpha||(1\,1\,1)_{M_{23}C_6}[1\,0\,0]_\alpha|||[0\,1\,\bar{1}]_{M_{23}C_6}$) orientation relationships were shown to hold between $M_{23}C_6$ and α-Fe. Generally, the stability and coarsening kinetics of the carbide particles depend significantly on their interface boundaries. However, there is no

*Corresponding author. Email: kipelova@bsu.edu.ru

information on the orientation relationships for $M_{23}C_6/\alpha$ during creep at elevated temperatures, although the coherency loss can lead to accelerated particle growth and to instability of the lath structure during creep and, therefore, reduce the creep strength.

The aim of the present study is to investigate the orientation relationships in a martensitic 9%Cr steel under conditions of tempering, aging and creep and to consider their effect on the stability of microstructure.

2. Experimental procedure

A 3%Co-modified P911-type steel (0.13%C, 8.6%Cr, 3.2%Co, 1.2%W, 0.9%Mo, 0.2% V, 0.1%Cu, 0.07%Nb, 0.06%Si, 0.05%Ni, 0.04%N, 0.02%Mn, 0.005%B, all in mass%, and the balance Fe) was investigated as a representative of an advanced martensitic creep resistant steels. The ingot was hot worked at 1100 °C to square bar of 25 mm × 25 mm. Then, the steel bar was austenitized at 1050 °C for 0.5 h followed by air cooling and tempered at 750 °C for 3 h. The creep tests were carried out at 650 °C with initial stress of 120 MPa. Microstructures of the specimens were examined using a JEM-2100 transmission electron microscope (TEM) operating at 200 kV. The aged and crept microstructures were observed on longitudinal sections of tested specimens in the grip, gauge and neck (1.5 mm away from the fracture surface) portions. Thin foils for TEM were prepared by double jet electro-polishing using a 10% solution of perchloric acid in glacial acetic acid. The carbides and their orientation relationships with matrix grains were identified by the selected area diffraction (SAD) method. At least 10 carbides were analyzed for each data point. The misorientations between (sub)grains were studied by the Kikuchi-line diffraction technique with low-angle converged beam [11]. The transverse lath/subgrain sizes were measured on the TEM micrographs by the line-crossing method. The dislocation densities were estimated by counting the individual dislocations revealed by TEM in lath/subgrain interiors. The simulation of coarsening behaviour of $M_{23}C_6$ carbides was performed using DICTRA26 software (mobility database MOB2, ThermoCalc Software). The details of calculations can be found elsewhere [12]. The stereographic projections were plotted by using Crystal Studio software.

3. Results and discussion

3.1. *Orientation relationships of $M_{23}C_6$ carbides after tempering and aging*

Typical tempered martensite lath structure of the P911 + 3%Co steel is shown in Figure 1. The microstructure consists of martensite laths with the transverse size of about 360 nm, which contain a rather high dislocation density of about 6.2×10^{14} m^{-2} in their interiors. The tempered martensite lath structure is characterized by a dispersion of $M_{23}C_6$ carbides. Almost all $M_{23}C_6$ carbides are located at grain/subgrain boundaries including prior austenite, packet, block and lath boundaries. The $M_{23}C_6$ particles exhibit slightly elongated shape along the boundary planes, and their average size is ~120 nm.

It can be seen from the SAD patterns in Figure 1(a) that $(1\,1\,0)_\alpha$ is parallel to $(1\,1\,1)_{M_{23}C_6}$. The beam direction for the $M_{23}C_6$ carbide is $[0\,1\,\bar{1}]_{M_{23}C_6}$, whereas the ferrite zone axes are $[1\,\bar{1}\,\bar{1}]_\alpha$ and $[0\,0\,\bar{1}]_\alpha$. Therefore, the orientation relationships can be written as:

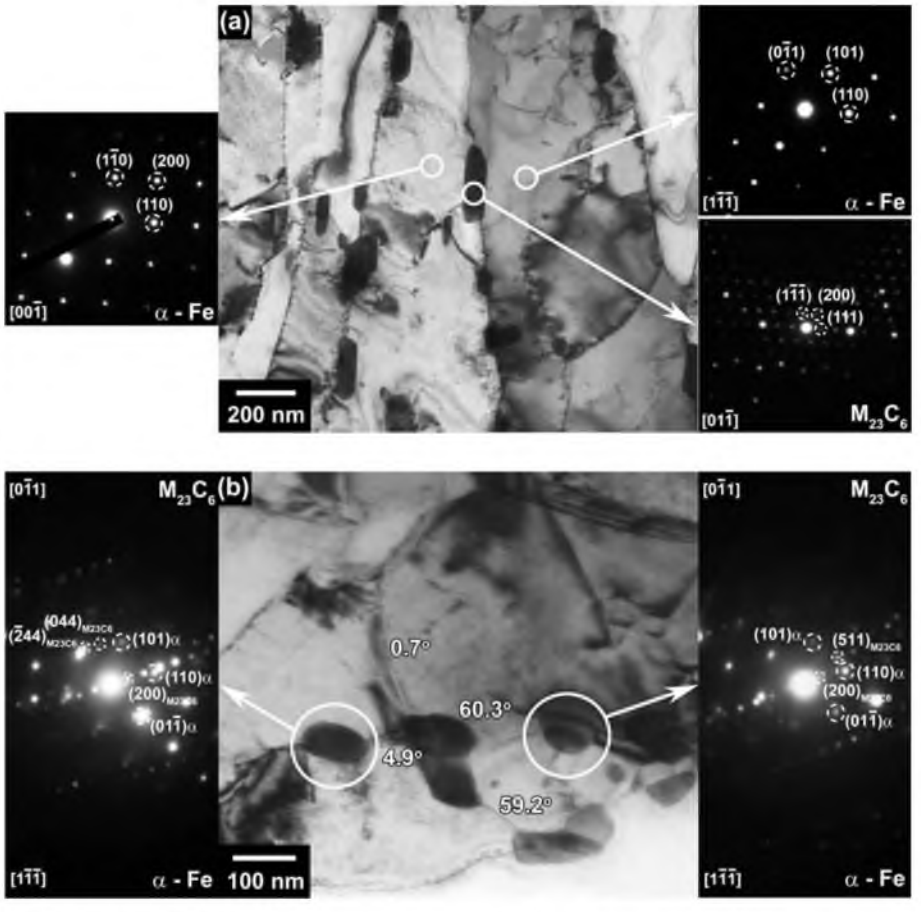

Figure 1. Microstructure of the tempered P911 + 3%Co steel and the SAD patterns from the $M_{23}C_6$ carbides and α-Fe, showing the orientation relationships.

$$(1\,1\,0)_{\alpha}||(1\,1\,1)_{M_{23}C_6}[1\,\bar{1}\,\bar{1}]_{\alpha}||[0\,1\,\bar{1}]_{M_{23}C_6} \tag{1}$$

$$(1\,1\,0)_{\alpha}||(1\,1\,1)_{M_{23}C_6}[0\,0\,\bar{1}]_{\alpha}||[0\,1\,\bar{1}]_{M_{23}C_6} \tag{2}$$

Those are the well known the Kurdjumov-Sachs and Nishiyama-Wassermann orientation relationships, respectively [10].

Figure 1(b) shows the composite electron diffraction patterns from two of the $M_{23}C_6$ carbides and the adjacent ferrite matrixes. The results suggest that $(1\,1\,0)_{\alpha}$ is parallel to $(2\,0\,0)_{M_{23}C_6}$, while $[1\,\bar{1}\,\bar{1}]_{\alpha}$ is parallel to $[0\,\bar{1}\,1]_{M_{23}C_6}$. Therefore, the following orientation relationship exists:

$$(1\,1\,0)_{\alpha}||(2\,0\,0)_{M_{23}C_6}[1\,\bar{1}\,\bar{1}]_{\alpha}||[0\,\bar{1}\,1]_{M_{23}C_6} \tag{3}$$

This is the well-known Pitsch orientation relationship between bcc and fcc crystals [13]. It should be noted that the analyzed $M_{23}C_6$ carbides are located at different boundaries. For instance, at the left of the Figure 1(b), the carbide is situated at low-angle boundary; the other carbide locates at high-angle boundary. Thus, the revealed orientation relationships are valid for $M_{23}C_6$ carbides precipitated at lath, block and packet martensite boundaries.

Also, two new crystallographic orientation relationships are found between α-Fe and $M_{23}C_6$. Figure 2 shows the electron diffraction patterns from the $M_{23}C_6$ carbide and the adjacent ferrite matrixes. The $(1\,1\,1)_{M_{23}C_6}$ plane is parallel to the $(1\,1\,0)_\alpha$, while the $[4\,\bar{3}\,\bar{1}]_{M_{23}C_6}$ zone-axis of carbide coincides with the ferrite zone axes of $[0\,0\,1]_\alpha$ and $[1\,\bar{1}\,\bar{1}]_\alpha$. Hence, the orientation relationships are the following:

$$(1\,1\,0)_\alpha \| (1\,1\,1)_{M_{23}C_6} [0\,0\,1]_\alpha \| [4\,\bar{3}\,\bar{1}]_{M_{23}C_6} \tag{4}$$

$$(1\,1\,0)_\alpha \| (1\,1\,1)_{M_{23}C_6} [1\,\bar{1}\,\bar{1}]_\alpha \| [4\,\bar{3}\,\bar{1}]_{M_{23}C_6} \tag{5}$$

The corresponding minimum angle-axis pairs are $38.66° < 0.925;\ 0.355;\ 0.128 >$ and $41.05° < 0.956;\ 0.244;\ 0.160 >$ for (4) and (5) relations, respectively. In total, the five orientation relationships between ferrite matrix and $M_{23}C_6$ carbides are observed for the tempered microstructure of the P911 + 3%Co steel. The stereographic projections of these orientation relationships are shown in Figure 3. The all orientation relationships are relatively close to each other; the deviations are about 8° (Figure 3, Table 1). Note here, two new crystallographic orientation relationships (4) and (5) are most close to the Kurdjumov-Sachs orientation relationship (Table 1).

In the orientation relationships (4) and (5), planes of carbide and matrix are close-packed, but the directions are not close-packed. The high-index directions for carbide associated with these relationships are illustrated in Figure 4, where the close-packed planes are displayed. The calculated lattice misfits for the five orientation relationships

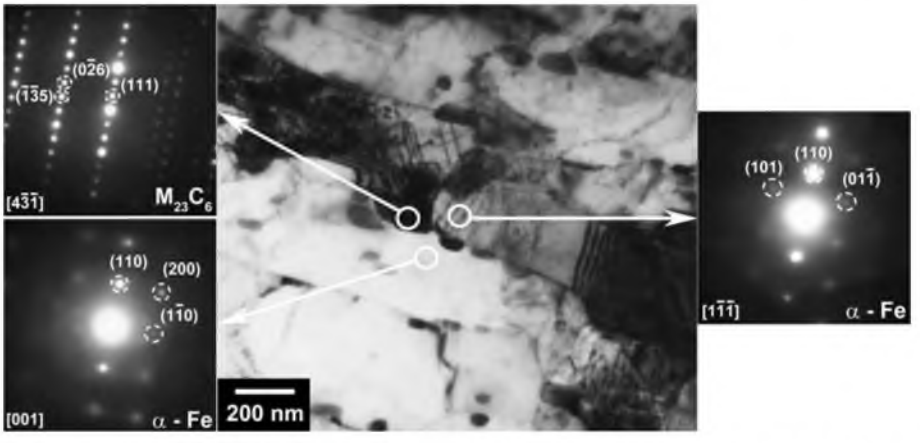

Figure 2. Microstructure of the tempered P911 + 3%Co steel and SAD patterns from the $M_{23}C_6$ carbide and α-Fe, showing the orientation relationships.

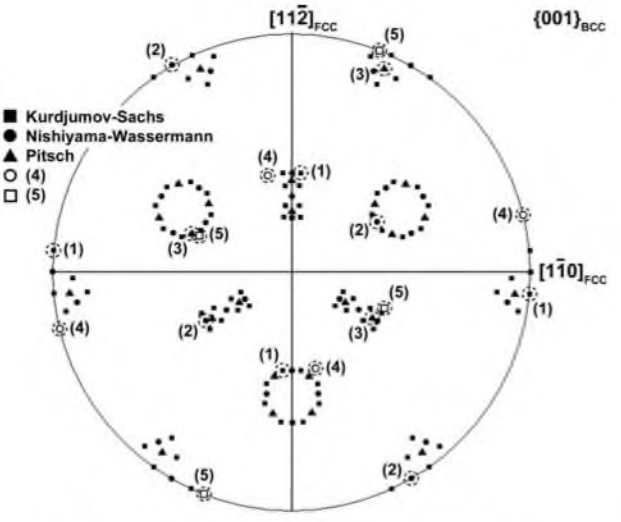

Figure 3. $\{100\}_{BCC}$ pole figure resulting from the low-index parallelism conditions projected onto the $(111)_{FCC}$ plane. The numbers correspond to the orientation relationship variants according to equations of 1–5.

Table 1. Deviations among the orientation relationships.

Orientation relationships	Kurdjumov-Sachs	Nishiyama-Wassermann	Pitsch
Kurdjumov-Sachs	0	5.3°	5.3°
Nishiyama-Wassermann	5.3°	0	7.4°
Pitsch	5.3°	7.4°	0
(4) $(1\,1\,0)_{\alpha}\|\|(1\,1\,1)_{M_{23}C_6}$ $[0\,0\,\bar{1}]_{\alpha}\|\|[4\,\bar{3}\,\bar{1}]_{M_{23}C_6}$	8.6°	13.2°	10.1°
(5) $(1\,1\,0)_{\alpha}\|\|(1\,1\,1)_{M_{23}C_6}$ $[1\,\bar{1}\,\bar{1}]_{\alpha}\|\|[4\,\bar{3}\,\bar{1}]_{M_{23}C_6}$	3.4°	8.6°	6.3°

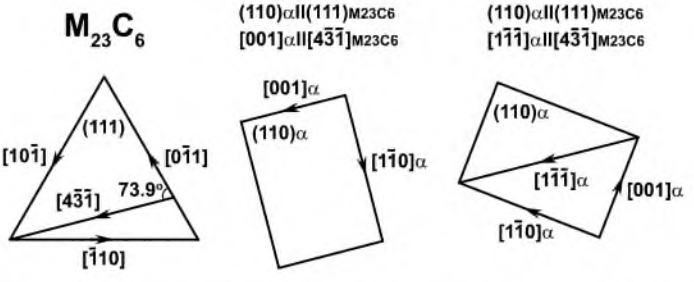

Figure 4. Alignment of crystallographic planes and directions in the α and $M_{23}C_6$ crystals for the (4) and (5) orientation relationships.

between ferrite matrix and $M_{23}C_6$ carbides, which are observed for the tempered microstructure of the steel, are listed in Table 2. The lattice misfit (δ) between $M_{23}C_6$ and α-Fe is defined by:

Table 2. Lattice misfits between ferrite matrix and $M_{23}C_6$ carbides.

Orientation relationships	$(hkl)_\alpha \| (hkl)_{M_{23}C_6}$	Lattice misfit (%)
(1) Kurdjumov-Sachs	$(1\,1\,0)_\alpha \| (3\,3\,3)_{M_{23}C_6}$	1.1
	$(2\,2\,2)_\alpha \| (10\,10\,0)_{M_{23}C_6}$	8.9
	$(2\,1\,1)_\alpha \| (8\,4\,4)_{M_{23}C_6}$	7.1
(2) Nishiyama-Wassermann	$(1\,1\,0)_\alpha \| (3\,3\,3)_{M_{23}C_6}$	1.1
	$(2\,0\,0)_\alpha \| (6\,6\,0)_{M_{23}C_6}$	12.4
	$(1\,1\,0)_\alpha \| (4\,2\,2)_{M_{23}C_6}$	7.3
(3) Pitsch	$(1\,1\,0)_\alpha \| (6\,0\,0)_{M_{23}C_6}$	12.4
	$(2\,2\,2)_\alpha \| (10\,10\,0)_{M_{23}C_6}$	8.9
	$(2\,1\,1)_\alpha \| (6\,6\,0)_{M_{23}C_6}$	7.3
(4) $(1\,1\,0)_\alpha \| (1\,1\,1)_{M_{23}C_6} [0\,0\,1]_\alpha \| [4\,\bar{3}\,-\bar{1}]_{M_{23}C_6}$	$(1\,1\,0)_\alpha \| (3\,3\,3)_{M_{23}C_6}$	1.1
	$(2\,0\,0)_\alpha \| (8\,6\,2)_{M_{23}C_6}$	27
	$(3\,3\,0)_\alpha \| (4\,10\,14)_{M_{23}C_6}$	10.8
(5) $(1\,1\,0)_\alpha \| (1\,1\,1)_{M_{23}C_6} [1\,\bar{1}\,\bar{1}]_\alpha \| [4\,\bar{3}\,\bar{1}]_{M_{23}C_6}$	$(1\,1\,0)_\alpha \| (3\,3\,3)_{M_{23}C_6}$	1.1
	$(2\,2\,2)_\alpha \| (8\,6\,2)_{M_{23}C_6}$	26.2
	$(4\,2\,2)_\alpha \| (4\,10\,14)_{M_{23}C_6}$	3.0

$$\delta = \frac{d_{M_{23}C_6} - d_\alpha}{d_\alpha} \tag{6}$$

where $d_{M_{23}C_6}$ and d_α are the interplanar spacing of $M_{23}C_6$ and α-Fe, respectively. It is clear that at least one α-Fe plane exhibits good coincidence (about 1% misfit) with the carbide lattice for all the orientation relationships except the Pitsch relationship, which is characterized by approximately 10% misfit along all three orthogonal planes. The well coincident planes are $(110)_\alpha$ and $(1\,1\,1)_{M_{23}C_6}$. It is seems that these coincident planes control the orientation relationship under condition that at least one of the other planes have a misfit of about 10%.

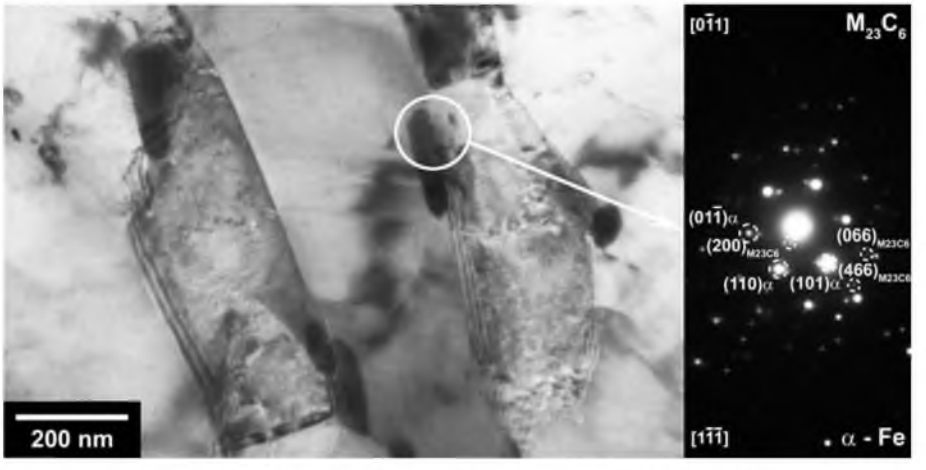

Figure 5. Microstructure of the P911 + 3%Co steel after aging for 4743 h and composite electron diffraction patterns from the $M_{23}C_6$ carbide and the adjacent ferrite matrix, showing the orientation relationship.

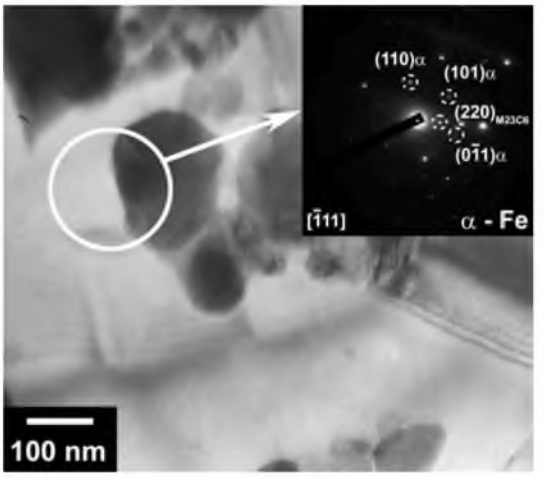

Figure 6. Microstructure and SAD patterns from the $M_{23}C_6$ carbide and α-Fe of the P911 + 3% Co steel after creep test to strain of 6%.

The previously reported low values of interfacial energy for $M_{23}C_6$ [3,8] and the revealed orientation relationships between ferrite matrix and $M_{23}C_6$ carbides in the present work indicate that the carbides are strongly bonded to matrix. Therefore, the $M_{23}C_6$ carbides are effective in pinning (sub)grain boundaries.

Representative micrograph of the microstructure in the grip portion of the sample subjected to creep test for about 4743 h is shown in Figure 5. In spite of the rather long-time exposure at elevated temperature, the microstructure in the grip portion looks similar to the initial tempered martensite lath structure. The structural changes are characterized by a small-scale growth of laths (the transverse lath size is ~500 nm) and the double reduction in dislocation density. The $M_{23}C_6$ carbides are located at (sub)grain boundaries. The mean particle size of $M_{23}C_6$ remained almost unchanged (~125 nm). The five aforementioned orientation relationships between ferrite matrix and $M_{23}C_6$ carbides retain during aging.

3.2. *$M_{23}C_6$ carbides after creep tests*

In contrast to the microstructures in the grip portion, the developed microstructures after creep tests to a strain of 6% and to rupture are quite different from the original tempered martensite lath structure (Figures 6 and 7). After creep test to a strain of 6%, the $M_{23}C_6$ carbides begin to lose their original orientation relationships with the α-Fe (Figure 6). Note here that 6% creep corresponds to the transition from the steady state creep to the accelerated creep [14]. A gradual disruption of the orientation relationships is accompanied by particle and subgrain coarsening. Thus, the original tempered martensite lath structure lost its lath morphology in the necking portion, where large plastic strain took place. The crept microstructure evolved in the neck portion looks like ordinary hot-worked microstructure consisting of subgrains, which are elongated along the plastic flow. The subgrain size of about 1300 nm remarkably exceeds the thickness of the original laths. It should be noted that an increase in the size of substructural

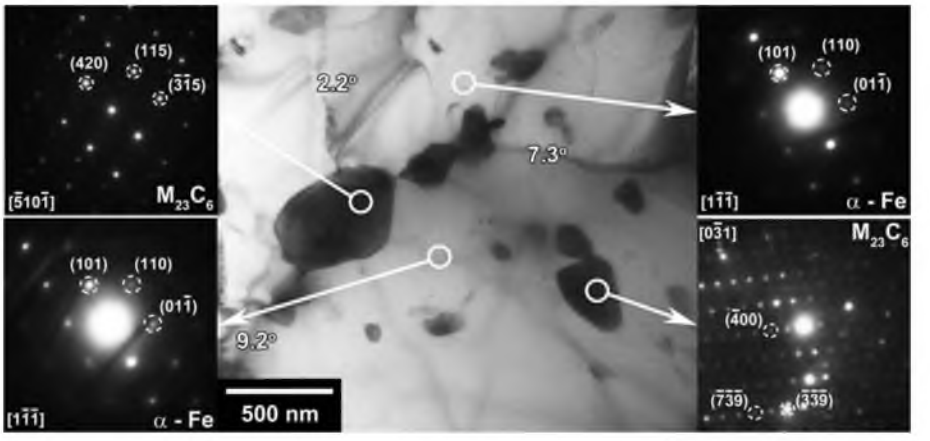

Figure 7. Microstructure and SAD patterns from the $M_{23}C_6$ carbides and α-Fe of the P911 + 3% Co steel after creep test.

elements clearly correlates with a decrease in the dislocation density from 6.2×10^{14} m^{-2} to 0.5×10^{14} m^{-2}. The $M_{23}C_6$ carbides exhibit almost equiaxial shape and are characterized by quite homogeneous distribution after the creep test; their average size increases to 214 nm. The $M_{23}C_6$ carbides lose their original orientation relationships with the α-Fe (Figure 7). The parallelism conditions for $M_{23}C_6/\alpha$ relations in Figure 7 can be written as:

$$(1\,1\,0)_{\alpha}||(739)_{M_{23}C_6}[1\,\bar{1}\,\bar{1}]_{\alpha}||[0\,\bar{3}\,1]_{M_{23}C_6} \tag{7}$$

$$(1\,1\,0)_{\alpha}||(115)_{M_{23}C_6}[1\,\bar{1}\,\bar{1}]_{\alpha}||[\bar{5}\;1\;0\;\bar{1}]_{M_{23}C_6} \tag{8}$$

The progressive deviation from original orientation relationships of $M_{23}C_6$ and α-Fe during creep is associated with strain incompatibilities at the interface boundaries. The hardness of the $M_{23}C_6$ carbides is significantly higher than that of the matrix [15,16]. If a deforming matrix contains non-deformable particles, a local strain incompatibility can be accommodated by the generation of geometrically necessary dislocations at the particle–matrix interface [17] as dislocation loops [18]. During creep, the accumulation of geometrically necessary dislocations at the particle–matrix interface leads to appearance of additional misorientation associated with dislocation arrays around a particle, which can be adequately described in terms of low-angle boundaries [17]. As a result, a rotation of the $M_{23}C_6$ carbides [18] takes place and the interface boundary energy per unit area increases.

Figure 8 shows the results of coarsening calculations for $M_{23}C_6$ particles with different interfacial energies (σ). The experimental data for the tempered and crept samples are used as reference points in the calculations. The σ values of 0.02 and 0.45 J/m^2 for coherent and incoherent interfaces, respectively, provide the best agreement with the experimental data. It is clearly seen in Figure 8 that the incoherent particles coarsen much faster than coherent ones. In turn, an increase in particle size is accompanied with a degradation of pinning force. Therefore, the mobility of (sub)grain boundaries

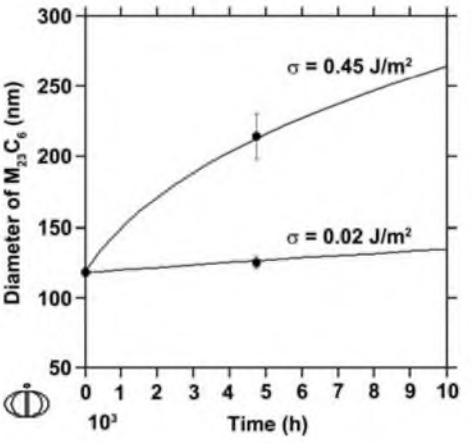

Figure 8. Coarsening of $M_{23}C_6$ in the P911 + 3%Co steel at 650 °C with $\sigma = 0.02\,J/m^2$ and $\sigma = 0.45\,J/m^2$. The circle symbols indicate the experimental values obtained by TEM measurements.

increases, leading to a significant coarsening of the tempered martensite lath structure. It can be concluded that the remarkable structural changes in the neck portion of crept specimen are caused by plastic relaxation in matrix at $M_{23}C_6$ particles by the generation of dislocation loops at interfaces [17,18], which, as a result, lose their coherency.

4. Conclusions

The orientation relationship of $M_{23}C_6$ carbides precipitated in a 3%Co-modified P911 heat-resistant steel was studied under conditions of tempering, aging and creep. The main results can be summarized as follows.

(1) Five orientation relationships between the $M_{23}C_6$ carbides and ferrite matrix were observed after tempering. Besides the Kurdjumov-Sachs, Nishiyama-Wassermann and Pitsch orientation relationships between bcc and fcc lattices, two new relationships are revealed: $(1\,1\,0)_\alpha||(1\,1\,1)_{M_{23}C_6}[0\,0\,1]_\alpha||[4\,\bar{3}\,\bar{1}]_{M_{23}C_6}$ and $(1\,1\,0)_\alpha||(1\,1\,1)_{M_{23}C_6}[1\,\bar{1}\,\bar{1}]_\alpha||[4\,\bar{3}\,1]_{M_{23}C_6}$.

(2) The orientation relationships between ferrite matrix and $M_{23}C_6$ carbides are disturbed during creep. The disruption of orientation relationships upon plastic flow increases the mobility of (sub)grain boundaries, leading to a significant coarsening of tempered martensite lath structure.

Acknowledgements

The study was supported by Department of Education and Science, Russian Federation, grant No. 02.523.12.3019. Authors are grateful to the staff of Joint Research Centre, Belgorod State University, for their assistance with structural and mechanical characterizations.

References

[1] M. Hattestrand, M. Schwind and H.O. Andren, Mater. Sci. Eng. A250 (1998) p.27.
[2] P.J. Ennis and A. Czyrska-Filemonowicz, Oper. Maint. Mater. 1 (2002) p.1.
[3] J. Hald and L. Korcakova, ISIJ Int. 43 (2003) p.420.
[4] B. Sonderegger, S. Mitsche and H. Cerjak, Mater. Sci. Eng. A481–482 (2008) p.466.
[5] M. Taneike, K. Sawada and F. Abe, Metall. Mater. Trans. 35A (2004) p.1255.
[6] K. Maruyama, K. Sawada and J. Koike, ISIJ Int. 41 (2001) p.641.
[7] H.G. Armaki, R. Chen, K. Maruyama and M. Igarashi, Metall. Mater. Trans. A42 (2011) p.3084.
[8] A. Gustafson and M. Hattestrand, Mater. Sci. Eng. A333 (2002) p.279.
[9] K.H. Kuo and C.L. Jia, Acta Metall. 33 (1985) p.991.
[10] P.R. Howell, J.V. Bee and R.W.K. Honeycombe, Metall. Trans. 10A (1979) p.1213.
[11] D.B. Williams and C.D. Carter, *Transmission Electron Microscopy*, Plenum Press, New York, NY, 1996.
[12] A. Kipelova, M. Odnobokova, A. Belyakov and R. Kaibyshev, Metall. Mater. Trans. A 44 (2013), p.577..
[13] Y. He, S. Godet and J.J. Jonas, J. Appl. Cryst. 39 (2006) p.72.
[14] A. Kipelova, A. Belyakov and R. Kaibyshev, Mater. Sci. Eng. A532 (2012) p.71.
[15] S. Shi, J.C. Lippold and J. Ramirez. *Repair weldability of service-exposed, heat-resisting alloys-austenitic stainless steel castings: HP45Nb, HP50Nb and 20–32Nb, Trends in Welding Research VII, Proc. of the 7th International Conference, ASM International* (2006) p. 293.
[16] M. Dumovic, Welding Innovation 20 (2003) p.2.
[17] M.F. Ashby, Philos. Mag. 21 (1970) p.399.
[18] F.J. Humphreys and M. Hatherly, *Recrystallization and related annealing phenomena*, Elsevier, Oxford, 2004.